EURASIAN PHYSICAL TECHNICAL JOURNAL

2025, Volume 22, No. 4(54)

https://doi.org/10.31489/2025N4/82-93

Received: 16/09/2025 Revised: 27/10/2025 Accepted: 22/12/2025 Published online: 29/12/2025

Research Article

UDC 53.083.7:621.396

MODELING AND MEASUREMENT OF ANTENNA CHARACTERISTICS OF A SATELLITE STATION BASED ON SOFTWARE-DEFINED RADIO

Baktybekov K.S.[1]*, Ashurov A. E.[2], Ivanov, A. V.[1], Kelgenbayev, A. Zh.[1], Zhapanova, A. S.[3], Sailaubaiuly S.[1]

[1] Ghalam LLP, Astana, Kazakhstan

[2] L.N. Gumilyov Eurasian National University, Astana, Kazakhstan

[3] S. Seifullin Kazakh Agrotechnical Research University, Astana, Kazakhstan

*Corresponding author: k.baktybekov@ghalam.kz

Abstract. *This study investigates the characteristics of a parabolic satellite antenna designed for communication with low Earth orbit satellites in the S-band. The choice of the S-band is motivated by the significantly lower power consumption of the radio link compared to the X-band. The S-band (2–4 GHz) is less sensitive to adverse weather effects than the X-band (8–12 GHz). These factors are critical for nanosatellites during Earth observation (EO) data transmission. Particular attention is given to measurements of the radiation pattern of the parabolic antenna in the S-band. These measurements provide essential data for optimizing the antenna design and parameters, thereby enhancing the overall efficiency of the communication system. During testing, both simulated and experimental radiation patterns of the gain were obtained, along with key antenna parameters such as Equivalent Isotopically Radiated Power, Input Power Flux Density, and the Gain-to-Noise Temperature Ratio. A comparison between measured and calculated results, including measurement accuracy and error budgets, demonstrated good agreement.*

Keywords: radiation pattern, parabolic antenna, S-band, ground station, gain measurement, modeling.

1. Introduction

Modern low Earth orbit (LEO) satellite systems play a crucial role in the development of global communication networks, offering low latency and high throughput, which are particularly valuable in applications such as the Internet of Things (IoT), Earth observation, and broadband access [1-2]. However, effective communication with rapidly moving LEO satellites requires antenna systems with high directivity that can adapt to dynamically changing link geometries. Parabolic antennas remain one of the most widely used solutions for ground stations due to their ability to focus electromagnetic energy into a narrow beam, ensuring high gain and minimal losses [3]. The main challenges in operating with LEO satellites are related to continuous tracking and compensation of atmospheric distortions, particularly in the X-band (8-12 GHz), where weather effects become significant [4]. In contrast, the S-band (2-4 GHz) is less affected by precipitation but requires a larger aperture size to achieve comparable directivity, complicating mechanical control [5]. Previous studies [6-7] have highlighted the importance of optimizing the reflector shape and feed system to minimize sidelobe levels, which is critical for reducing interference in dense satellite constellations.

Modern approaches to enhancing the efficiency of parabolic antennas include hybrid solutions that combine mechanical scanning with electronic beam steering using phased arrays [8]. However, as noted in [9],

most research has been focused on geostationary satellites, while the specific challenges of LEO orbits-such as short visibility windows and frequent beam reorientation-remain insufficiently explored. This paper presents a comprehensive analysis of the directional characteristics of a parabolic antenna in the S-band, including radiation pattern modeling, gain evaluation, and both simulation and measurement of Equivalent Isotropically Radiated Power (EIRP), Input Power Flux Density (IPFD), and the Gain-to-Noise Temperature Ratio (G/T). The results are compared with recent studies on adaptive algorithms [10], providing recommendations for the design of next-generation ground stations.

In recent years, significant attention has been devoted to optimizing the directional characteristics of parabolic antennas for LEO satellites. Research indicates that in the X-band, achieving a gain of 50–55 dBi requires extremely high reflector surface accuracy (RMS ≤ 0.25 mm) and careful feed design [11]. In the S-band, however, challenges remain in reducing cross-polarization distortions and adapting to varying satellite orientations, which is often addressed through circular polarization [12]. It was also shown in [12] that a developed software-defined radio (SDR) transceiver based on field-programmable gate arrays (FPGA) provides greater flexibility, enabling operation across multiple frequency bands, filtering schemes, and adaptive modulation and coding techniques without major hardware modifications.

Within this research, both radiation pattern modeling and gain evaluation were carried out, and the results were compared against experimental measurements. Particular emphasis was placed on measuring the radiation pattern of the parabolic antenna in the S-band, designed for receiving payload data and telemetry as well as transmitting command signals. These measurements provide essential insights for optimizing antenna design and parameters, thereby improving the overall performance of the communication system.

2. Structural scheme of the device under test and radiation pattern simulation results

The device under test is a prime-focus parabolic reflector antenna developed for operation in the frequency range 2.025 - 2.300 GHz with right- and left-hand circular polarizations. The parabolic reflector has a diameter of 3.7 meters and is equipped with a dual-band waveguide feed. The dual-band feed is installed at the prime focus of the reflector and provides simultaneous reception in the X-band as well as both transmission and reception in the S-band [13]. The S-band receive chain includes a low-noise amplifier (LNA) with a gain of 30 dB at 2.226 GHz for downlink (DL) and 2.060 GHz for uplink (UL). For measurement purposes, a test coupler (BDC 1018-30/20S, S-band downlink) was added to the scheme.

The bandpass filter, directional coupler, and LNA are integrated into the feed assembly. The LNA is powered via a supply unit located in the enclosure assembly (downlink). A test cable is routed between the output of the power supply and the switch on the DUT positioner. The modem unit is a functional subsystem that consists of an SDR modem and a control computer. The SDR performs the primary signal processing tasks-modulation, demodulation, filtering, and frequency conversion. The control computer operates the SDR, implements communication protocols, processes data, and provides interfacing with external systems [13].

The S-band transmit chain (enclosure assembly uplink), including a preamplifier and a high-power amplifier (HPA) with an output power of 30 W, amplifies the RF signal generated by the SDR. The amplified signal is transmitted through the chain with consideration for circular cross-polarization isolation (S-band uplink). The signal is then fed into the antenna feed and radiated by the antenna at 2060 MHz. The structural scheme of the testing device is shown in Figure 1.

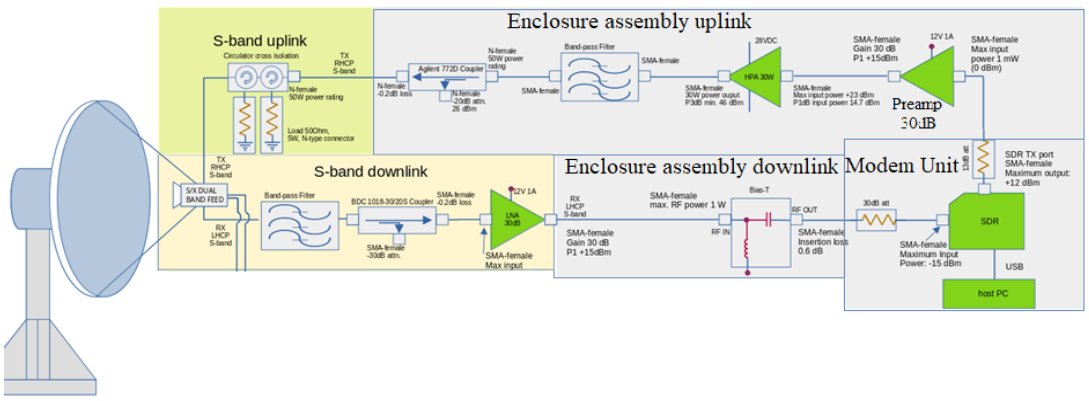

Fig.1. Structural scheme of testing device.

Prior to testing, the antenna geometry was modeled in CAD, and simulations were conducted in Ansys HFSS. The calculated radiation pattern of the antenna in the S-band at 2060 MHz is presented in Figure 2.

The contour plot of the calculated radiation pattern of the antenna in the S-band at 2060 MHz is shown in Figure 3.

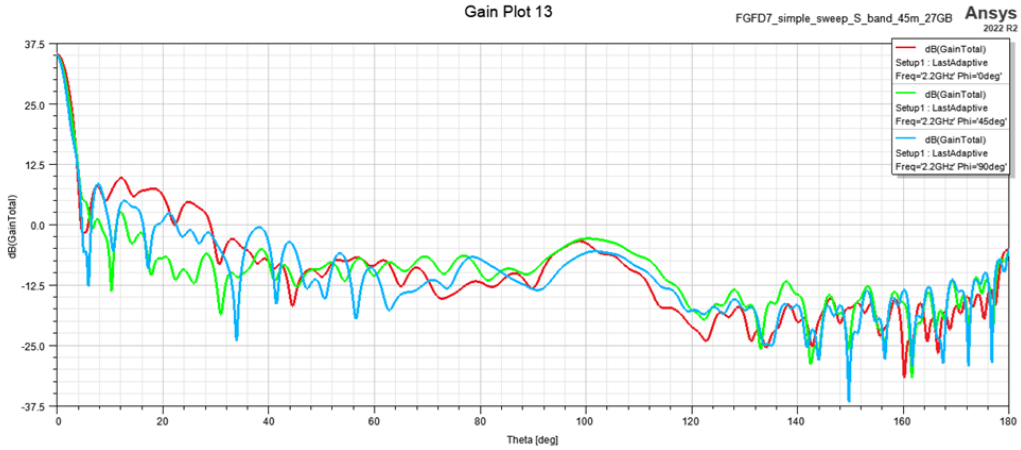

Fig.2. Calculated radiation pattern of the antenna in the S-band.

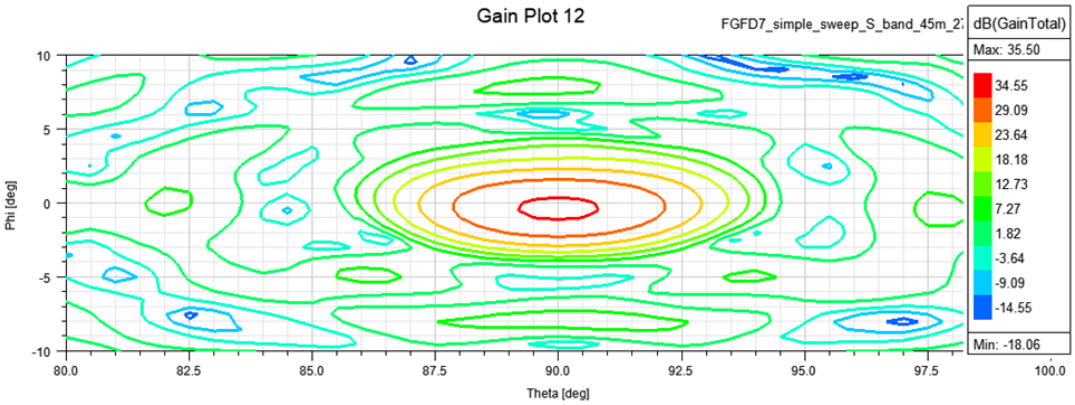

Fig.3. Contour plot of the calculated radiation pattern of the antenna in the S-band.

According to the modelling results in ANSYS HFSS, the antenna Gain should be 35.5dBi maximum, and beamwidth around 2.5 degrees at -3dB. Side-lobes are at level -25dB.

3. Antenna radiation pattern measurements

The radiation pattern measurements were performed using the "on-the-fly" method, in which the measurement axis (AZ or EL) of the DUT positioner is continuously scanned over a predefined angular range without stopping at each grid point. The measurement is conducted during the motion sequence when the DUT positioner passes through one of the specified grid points. The applied DUT positioner supports radiation pattern measurements in both receive (DL) and transmit (UL) modes, enabling a comprehensive analysis of antenna characteristics. For the present study, the antenna radiation pattern was measured in receive mode.

The RF budget of the antenna radiation pattern at 2.226 GHz is presented in Table 1. The experimental setup for radiation pattern measurement is shown in Figure 4. The test setup for radiation pattern measurements consists of three sections: the Feed room, Measurement room, and Operator room. Each section represents a dedicated space housing specific equipment. The Feed room includes the feed positioner 30R99 and the equipment rack 30R01. The Measurement room contains the DUT positioner 10R99 and equipment racks 10R01 and 10R02. The Operator room hosts the equipment rack 20R01 and the operator's workstation.

The transmit subsystem comprises an RF synthesizer (1) located in rack 30R01, as well as power amplifiers (2), a broadband directional coupler (5), and a PIN switch (6). The latter is used to switch between two linear polarization ports of the feed (7) and operates up to 40 GHz (30R99). Port switching is controlled

by the measurement system controller (13) and PC1 software. The receiver (13), controller (14), and PC1 are installed in the Operator room. A frequency distribution converter, Mixer 1 (3), is located in the Feed room (30R99) to handle the RF reference signal.

Table 1. RF budget of the antenna radiation pattern at 2.226 GHz

F, MHz	Gen out, dBm	Gen out-PA in, path loss, dB	HPA #1, gain dB	J05 F-Feed, dB	Tx feed, Gain, dBi	Free-space Loss, dB	Anten-na Gain, dBi	Filter, dB	DUT coupl-er, dB	DUT coupler-LNA in, loss, dB	ASCU LNA, input, dBm	LNA, gain, dB	Rx Mixer, dBm
2226	-30	-3,5	42	-1,5	12	-64,90	35	-1	-30	-4,5	-46,40	25,7	20,7

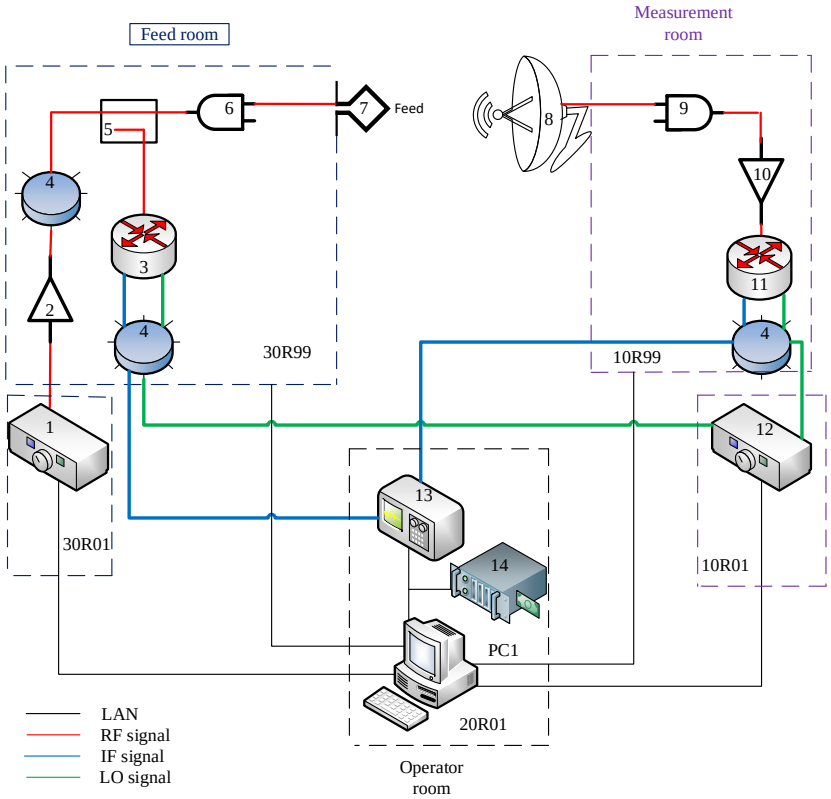

Fig.4. Experimental setup for radiation pattern measurement.

The RF signal is generated by the synthesizer, with frequency and power levels controlled at a fixed reference level using the microwave receiver (13) and PC software via the IEEE bus from PC1. The transmitted and amplified RF signal is radiated through the feed (7). Along the signal path, several coaxial switches are employed, including an IF switch block (4) for Tx/Rx mode selection. The reference signal coupler (5) is connected to the reference mixer Mixer 1 (3), which operates in the main mixing mode, ensuring extended dynamic range and thus higher measurement accuracy.

The receive subsystem consists of the antenna under test (8), a 2-port PIN switch (9), a low-noise amplifier (LNA) (10), Mixer 2 (11), coaxial IF switch block (4), and an LO synthesizer (12). The intermediate frequency signal from the IF switch is routed to port 2 of the receiver (13), where it is processed and read using the software on PC1. The system controller (14) performs synchronization, distributing trigger pulses from the position encoder to the measurement equipment (RF/LO sources, receiver, and PIN switches) as the DUT passes through the specified points, ensuring precise timing coordination of the measurements.

4. Antenna Gain Measurements

The application of the three-antenna gain measurement methods is generally infeasible due to the large size of the antenna and the limited space in the feed room. Furthermore, the antenna's dimensions do not allow for disassembly or replacement with other antennas on the feed positioner, which is required for applying the three-antenna techniques. Therefore, the power measurement method (PMM) [14] was employed in the experimental setup. This method is well established and widely used. Determining the gain with a power meter is both flexible and efficient, making it particularly suitable for large satellite antennas. The described method provides a measurement accuracy of ±0.25 dB.

In the measurement software was added gain measurement method utilizing two power sensor heads. This enables measurements of the absolute gain of the DUT. By measuring the output power of the feed, the input power of the antenna, and accounting for free-space losses as well as the feed gain, the gain of the device under test can be readily calculated using the following equation:

$$\frac{P_r}{P_t} = \left(\frac{\lambda}{4\pi R}\right)^2 \cdot G_t \cdot G_r; \quad (1)$$

where: Pt - transmitted power; Pr - received power; Gt - transmitting antenna gain; Gr - receiving antenna gain; R - free-space distance; λ - wavelength.

Table 2 presents the radio frequency (RF) link budget of the antenna gain at 2.226 GHz.

Table 2. Radio frequency (RF) link budget of the antenna gains at 2.226 GHz.

F, MHz	Gen out, dBm	Gen out-HPA in path los, dB	HPA#1 Gain, dB	J05F-Feed, dB	Tx feed Gain, dBi	Free-space Loss, dB	Anten-na Gain, dBi	Filter, dB	DUT coupler, dB	DUT coup-ler LNA in, dB	ASCU LNA in, dBm	LNA Gain, dB	Rx Mixer, dB
2226	-38,5	-3,5	42	-6,4	12	-64,84	34	-1	-30	-4,5	-63,7	25,7	-38,04

Figure 5 shows the block diagram of antenna gain measurement in the receive mode (DUT Rx).

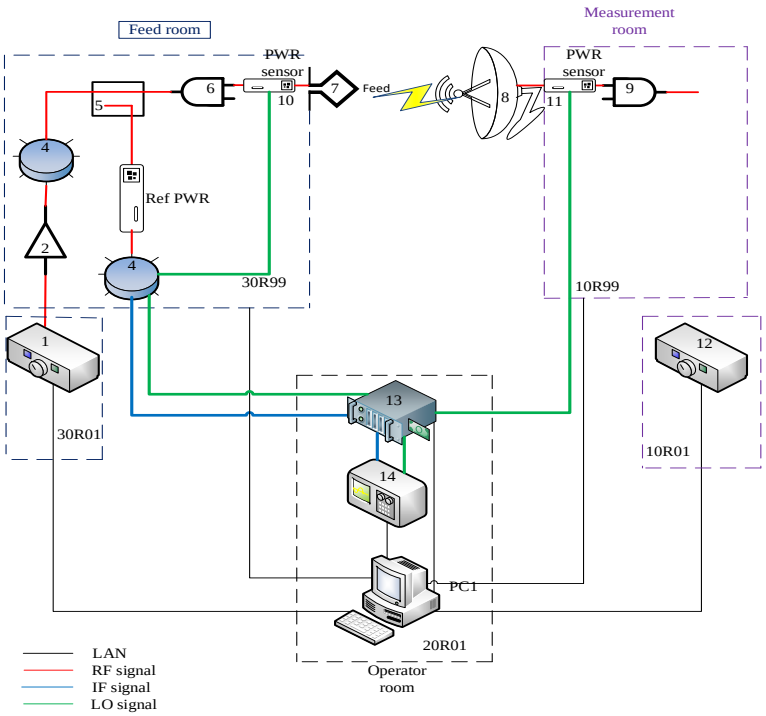

Fig.5. Block diagram of antenna gain measurement.

In this mode, the PC1 software, together with power sensors (10, 11) connected via the controller (13), provides automatic switching between power measurements at the input port (11), connected to the antenna (8), and the output port (10), connected to the feed (7). The measured power values from both ports are fed into the power meter (14) and then transferred via the IEEE interface to the personal computer (PC1), where they are processed by the software in accordance with the previously presented equation. The measured value of 31 dBi then should be corrected by adding 3dB due to the applied method and hardware. The measurement feeds are operating in linear polarization, whereas the DUT feed in circular. Therefore the resulted Gain is equal to 34 dBi.

5. Equivalent Isotropically Radiated Power (EIRP) Measurement

The Equivalent Isotropically Radiated Power (EIRP) is defined as the product of the transmitting antenna gain (G_{TX} in given direction and the input power applied to the antenna (P_{TX}):

$$EIRP = G_{TX} \cdot P_{TX} \quad (2)$$

For EIRP measurement, a formula based on the Friis transmission equation is applied, where the parameters of the range feed antenna are used instead of those of the device under test (Tx antenna):

$$EIRP = \frac{P_{RX,feed} \cdot LP_{down}}{G_{RX,feed}}; \quad (3)$$

$$LP_{down}=(4\pi R/\lambda)^2; \quad (4)$$

where: LP_{down}- free-space path loss, $G_{RX,feed}$- range feed gain; $P_{RX,feed}$ - received power at the range feed; λ - wavelength of the test signal; R - free-space distance (distance between the device under test and the range feed).

The RF budget of the EIRP at 2.060 GHz is presented in Table 3. The antenna must be aligned with the symmetry axis of the measurement zone (Measurement Room). The input signal is applied as a synthesized continuous wave (CW) (1) with a sufficient level to saturate the transponder (10R02). The transmitted and received power are measured using power meters (3) and (11), and based on the known antenna characteristics and the distance to the Range Feed antenna, the EIRP is calculated.

Table 3. RF budget of the EIRP at 2.060 GHz.

F, MHz	Prx (PM), dBm	Cable path D/L Loss, dB	D/L Range feed Gain, dBi	Free space Loss, dB	dBm to dBW	EIRP, dBW
2060	12,75	-6,4	11,6	-64,23	30	41,78

Note: EIRP and IPFD tests are typically performed under payload saturation conditions, i.e., at its maximum output power. Two methods are commonly used to determine saturation [15]:

- by measuring the maximum output power using power meters (3) and (11);
- by analyzing the carrier-to-noise ratio using the signal analyzer (9).

Figure 6 illustrates the schematic diagram for the EIRP test.

6. The Input Power Flux Density (IPFD) Measurement

The Input Power Flux Density (IPFD) is defined as the power flux density required to saturate the device under test, and can be expressed as [16]:

$$IPFD = P_{TX,feed} \cdot G_{TX,feed} \cdot \left(\frac{1}{4\pi R2}\right), \quad (5)$$

where: $G_{TX,feed}$ is the range feed gain; $P_{TX,feed}$ is the transmitted power of the range feed; R is the free-space distance (i.e., the distance between the device under test and the range feed); $(1/4\pi R^2)$ is the free-space distribution factor.

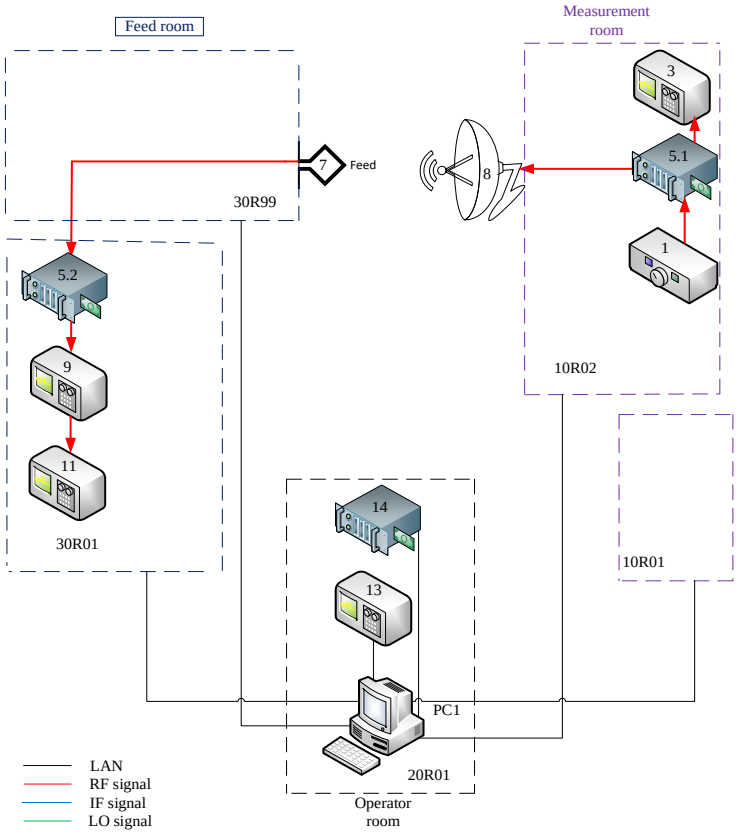

Fig.6. EIRP testing scheme.

The RF budget of the IPFD at 2.060 GHz is presented in Table 4. To determine the IPFD, the testing antenna (Measurement Room) must be aligned with the axis of the measurement zone at the maximum of its radiation pattern. A synthesized CW signal (1) is applied through the feed (7), ensuring saturation of the payload of the antenna (Measurement Room). The required input power saturation level at the antenna can be measured using the power meter (10). With the known feed gain and the distance **R**, the IPFD can then be calculated using the aforementioned equation in the PC1 software. Figure 6 presents the schematic diagram of the IPFD test.

Table 4. RF budget of the IPFD at 2.060 GHz.

F, MHz	Power Meter Tx, dBm	Cable path U/L reference, dB	Tx Power dBm	U/L cable path 7m loss, dB	U/L Range antenna gain, dBi	Spreading loss, dB	dBm to dBW	IPFD, dBW/m^2	IPFD circular estimation
2060	-36	-16	-20	-6	12	-36,44	30	-50,44	-53,44

7. Measurement of Receiver Chain Figure of Merit (G/T)

The principle of the test setup for G/T is shown in Figure 7. The determination of G/T is performed by measuring three different power levels [17]:

– P_1 - the noise power level of the receiving test equipment. For this purpose, the feed (7) is terminated with a 50 Ω load, and the test equipment (10R02) is disconnected from the antenna. The intrinsic noise of the test equipment P_1 (10) is then measured;

– P_2 - the noise power level of the receiving test equipment, including the internal noise of the measurement equipment (10R02);

– P_3 - the power level of the receiving test equipment (10R02), including the antenna noise and the power from the feed.

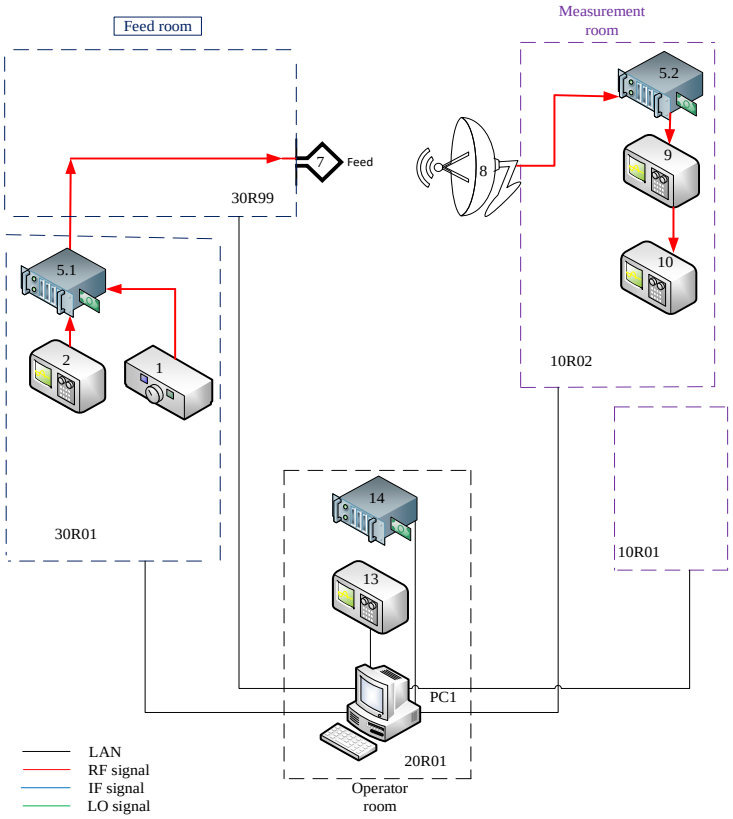

Fig.7. Schematic diagram of the IPFD and G/T test.

After the power levels are measured, the stored data are processed in the PC1 software, where the G/T value is automatically calculated using the following equation [18].

$$\frac{G}{T} = \left(\frac{k \cdot B * \cdot LP}{EIRP}\right) \cdot \left(\frac{P3-P2}{P2-P1}\right), \quad (6)$$

where: LP - is the free-space path loss; k - is the Boltzmann constant; B - is the resolution bandwidth.

Table 5. RF budget of G/T at 2.060 GHz.

F, MHz	Ptx, dBm	Cable path U/L, dB	U/L range antenna	EIRP Tx	Free space, dB	P1, dBm	P2, dBm	P3, dBm
2226	-40	-6	12	-34	-64,90	-49,8	-49,79	-39,38

Y1, dB	Y1 lin	Y1-1	Y2, dB	Y2 lin	Y2-1	k, dBW/Hz/K	k, dBm/Hz/K	NBW, Hz	NBW dBHz	G/T
0,01	1,00251	-26,5738	10,41	10,9901	9,99561	-226,6	-199,6	942000	59,74050901	-5,65884

8. Results and discussion of the experiment

The proposed system provides Fundamental RF mixing up to 18 GHz and then Low-Harmonic RF mixing (3rd harmonic) up to 40 GHz and therefore sufficient measurement speed, sensitivity and dynamic range

without the use of large amounts of coherent integration or very small IF bandwidths. Fundamental and Low-Harmonic mixing also minimizes the accuracy problems associated with RF and LO harmonics when measuring wide-band antennas. Due to the design of the Distributed Frequency Converter, and the internal design of the IF processing Unit, system stability and accuracy improve significantly. The system stability is a key factor in achieving high levels of measurement repeatability.

The excellent accuracy means antenna patterns can be measured over an extremely wide dynamic range with less than 0.1 dB of uncertainty due to the instrumentation.

The system uses an industrial standard measurement system in our modified configuration. A RF multiplexing is applied with the switches to extend the number of measurement channels. Only a single mixer (reference mixer type is used) is required, allowing use of a single rotary joint in the positioner. Furthermore, the sources and receiver are triggered using a TTL handshake, resulting in a higher frequency switching speed. The receiver operates in fast - CW mode and stores the measured data in its internal point buffer, from where it is transferred to the control computer in an asynchronous fashion. This configuration minimizes overhead and makes maximum use of the high speed of the individual components.

The graphs below present the results of the normalized three-dimensional radiation pattern (Fig. 8), the antenna gain (Fig. 9), and the normalized contour plot of the gain (Fig. 10).

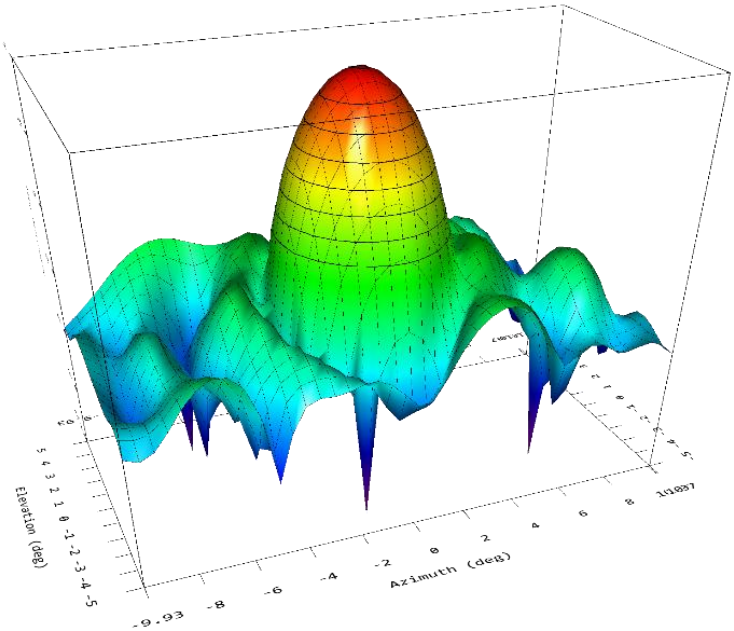

Fig.8. Three-dimensional radiation pattern.

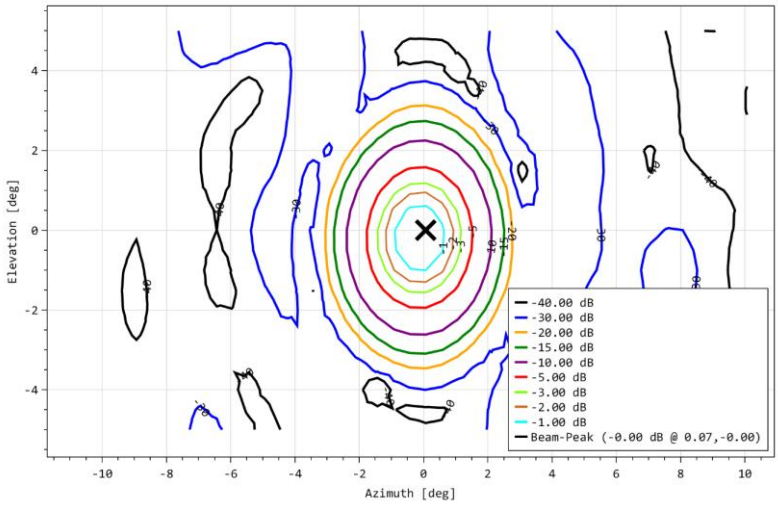

Fig.9. Contour graph of the gain.

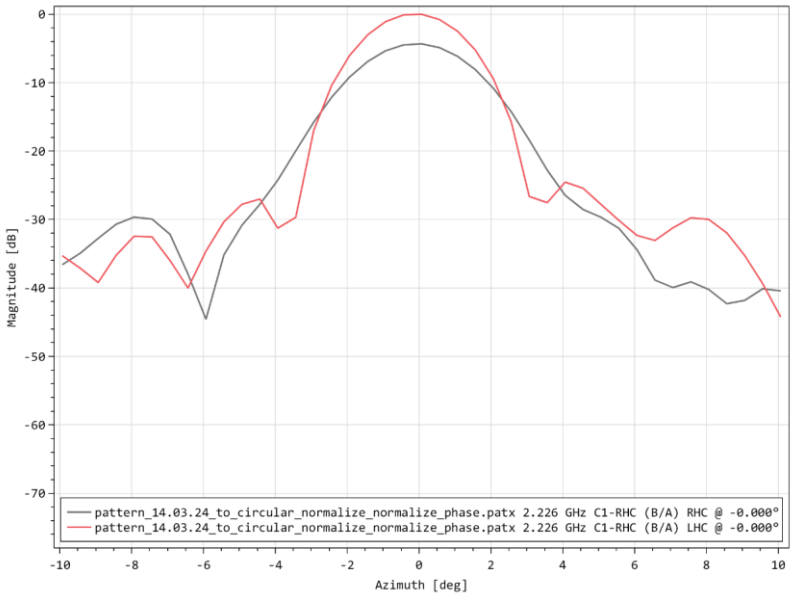

Fig.10. Antenna Gain versus Direction.

As seen from the plots, the pattern width at -3dB is around 2.4 degrees, which is very close to the expected from modelling (2.2 deg.). The total Gain of the tested antenna is 34 dBi, and side-lobes at level -25dB, which is very close to the expected value.

Overall, the observed results are consistent with the calculated values obtained from Ansys simulations. Minor discrepancies may be attributed to inaccuracies in the CAD model, as well as inaccuracy in manufacturing and fastening of the antenna feed to the reflector. The test results are presented below in Table 6. The test results show that the measured parameters of EIRP, IPFD, and G/T are generally consistent with the preliminary simulations. The most significant deviation is observed in the EIRP values, which requires further analysis to determine the reasons for exceeding the design specifications.

Table 6. Test results with payload.

DL Frequency / DL, MHz	UL Frequency / UL, MHz	Power Budget calculations			Measurement results		
		EIRP	IPFD	G/T	EIRP	IPFD	G/T
2220	2058	41.78	-50.44	-5.02	43.23	-50.32	-5.04
2226	2060	41.78	-50.44	-3.64	45.06	-50.1	-3.69
2230	2062	41.78	-50.44	-3.69	44.84	-50.17	-3.75

The IPFD and G/T parameters demonstrate a high degree of agreement with the calculated models, confirming the reliability of the receiving chain characteristics and the antenna's noise properties. These data can be further used for evaluating the compliance of the antenna and payload with the design requirements.

9. Conclusion

Tests of the S-band channel of the earth station's antenna system for receiving and transmitting signals from low Earth orbit (LEO) satellites were conducted. As part of the antenna and payload testing, procedures for measuring and collecting experimental data were developed. Namely, the proposed system achieves high accuracy, stability, and speed by combining Fundamental and Low-Harmonic RF mixing with an optimized Distributed Frequency Converter architecture. The modified industrial-standard setup provides increased channel capacity using RF multiplexing, while the minimized overhead and the maximized component speed are achieved through TTL triggered fast-CW data acquisition.

Accordingly, a CAD model of the parabolic antenna was created, and calculations of parameters such as equivalent isotropically radiated power (EIRP), input power flux density (IPFD), and the gain-to-noise-temperature ratio (G/T) were performed. Simulations were carried out in ANSYS HFSS. Experimental measurements of these parameters showed good agreement with the calculated results. These results indicate that the developed antenna system is ready for use in the satellite-communications earth station, and that the antenna test range is ready for further operation.

Conflict of interest statement

The authors declare that they have no conflict of interest in relation to this research, whether financial, personal, authorship or otherwise, that could affect the research and its results presented in this paper.

CRediT author statement

Baktybekov K.S.: Conceptualization, Supervision - Original Draft; **Ashurov A. E.:** Writing - Review & Editing; **Zhapanova, A.S.:** Data Curation – Writing; **Ivanov, A. V.:** Data Curation – Writing; **Kelgenbayev, Al. Zh.:** Writing – Review; **Sailaubaiuly S.:** Writing – Review. The final manuscript was read and approved by all authors.

Funding

This research has been/was/is funded by the Aerospace Committee of the Ministry of Digital Development, Innovations and Aerospace Industry of the Republic of Kazakhstan (BR 21982462)

References

1 Li Ye., Wang M., Hwang K., Li Z., Ji T. (2023) LEO Satellite Constellation for Global-Scale Remote Sensing with On-Orbit Cloud AI Computing. IEEE Transactions on Aerospace. *IEEE Journal of Selected Topics in Applied Earth Observations and Remote Sensing*, 16, 9369 – 9381. https://doi.org/10.1109/JSTARS.2023.3316298

2 Cedric Westphal, Lin Han, Richard Li. (2023) LEO satellite networking relaunched: Survey and current research challenges. *ITU Journal on Future and Evolving Technologies*, 4, 4, 711-744. https://doi.org/10.52953/LWXC1928

3 Manuel Arrebola., Leandro de Haro, Jose A Encina. (2008) Analysis of Dual-Reflector Antennas with a Reflectarray as Subreflector. *IEEE Antennas and Propagation Magazine*, 50, 6, 39 – 51. https://doi.org/10.1109/MAP.2008.4768921

4 Taeyoung Kim. (2024) An Analysis of Issues Related to Attenuation by Atmospheric Factors in the Frequency Bands for Radar Systems. *Journal of the Korean Military Science and Technology Society*, 27, N6, 657- 664. https://doi.org/10.9766/KIMST.2024.27.6.657

5 Dhanush S., Sreelakshmi K., Ranjit G., Dora K., Susarla Hari. (2023) LNA Design for LEO Space S-Band Applications. Proceeding of the 6th International Conference on Computation System and Information Technology for Sustainable Solutions (CSITSS), Bangalore, India. *IEEE Xplore*. https://doi.org/10.1109/CSITSS57437.2022.10026407

6 Rodrigues G., Angevain J.C, Santiago-Prowald J. (2013) Shape optimization of reconfigurable antenna reflectors. *CEAS Space J.*, 5, 221–232. https://doi.org/10.1007/s12567-013-0038-5

7 Evans G.E., Schrank H.E. (2024) A Planar Series-Feed Antenna Array with an Extremely Low Sidelobe Level. October 2024. *IEEE Antennas and Wireless Propagation Letters*,1 - 5. https://doi.org/10.1109/LAWP.2024.3483269

8 Rui Chen, Zhenyang Tian, Wen-Xuan Long, Xiaodong Wang, Wei Zhang (2023) Hybrid Mechanical and Electronic Beam Steering for Maximizing OAM Channel Capacity. *IEEE Transactions on Wireless Communications*, 22, 1, 534 - 549. https://doi.org/10.1109/TWC.2022.3195988.

9 Marco Lisi (2002) Phased arrays for satellite communications: a system engineering approach. *Proceedings of the 2000 IEEE International Conference on Phased Array Systems and Technology (Cat. No.00TH8510). IEEE Xplore*. https://doi.org/10.1109/PAST.2000.858938

10 Raúl Igual, Carlos Medrano, Inmaculada Plaza Carlos Orrite (2013) Adaptive tracking algorithms to improve the use of computing resources. *IET Computer Vision*, 7(6), 415 – 424. https://doi.org/10.1049/iet-cvi.2012.0016

11 Pedram Mousavi, Lotfollah Shafai, Veidt B., Dewdney P. (2001) Feed-Reflector design for large adaptive reflector antenna (LAR). *IEEE Transactions on Antennas and Propagation*, 49(8), 1142 – 1154. https://doi.org/10.1109/8.943309

12 Zhao P., Chen N., Li Y., Feng C. (2023) Cross-Polarization Interference Cancellation in Satellite Communication. *Proceedings of the 5th International Conference on Electronic Engineering and Informatics (EEI)*, Wuhan, China, 391 – 395. https://doi.org/10.1109/EEI59236.2023.10212784

13 Baktybekov K.S., Bochkova E.N., Korol V.V., Murushkin M.S., Zhumazhanov B.R. (2024) Design of Software Defined Radio of Ground Station for Receiving Nanosatellites Image Data in S-band. *Eurasian Physical Technical Journal*. 21, 4(50), 79 – 87. https://doi.org/10.31489/2024No4/79-87

14 Fasold D. (2006) Measurement Performance of Basic Compact Range Concepts. *Proceedings of the 21st Antenna Measurement Technical Association (AMTA)*, Europe, 2006. https://doi.org/10.1109/RAST.2015.7208382

15 Hunscher C., Hartmann J. (2007) Satellite Antenna Measurements. *Proceedings of the 2nd International ITG Conference on Antennas*, Munich, Germany, 25 – 32. https://doi.org/10.1109/INICA.2007.4353925

16 Velasco C., Tipantuña C. (2017) Meteorological picture reception system using software defined radio (SDR). *Proceeding of the IEEE 2nd Ecuador Technical Chapters Meeting*, 1-6. https://doi.org/10.1109/ETCM.2017.8247551

17 Farrar A. (1985) Computer Models for Determination of Satellite Power-Flux-Density Limits. *Proceeding of the 6th Symposium and Technical Exhibition on Electromagnetic Compatibility*. Zurich, Switzerland, 315 – 320. https://doi.org/10.23919/EMC.1985.10798853

18 Ohmaru K., Mikuni Y. (1984) Direct G/T Measurement for Satellite Broadcasting Receivers. *IEEE Transactions on Broadcasting*. BC-30, 2, 38 – 43. https://doi.org/10.1109/TBC.1984.266529

AUTHORS' INFORMATION

Baktybekov, Kazbek Suleimenuly - Doctor of Physical and Mathematical Sciences, Professor, Payload and Research Department, Research Associate, Ghalam LLP, Astana, Kazakhstan; Scopus Author ID:8926833000; https://orcid.org/0000-0002-6401-8053; k.baktybekov@ghalam.kz

Ashurov, Abdikul Erkulovich - PhD, Head of the Department of Space Engineering and Technology, L.N. Gumilyov Eurasian National University, Astana, Kazakhstan; Scopus Author ID: 57942248600; https://orcid.org/0000-0001-6044-5579 ; ashurov_ae@enu.kz

Ivanov, Anton Vladimirovich – Engineer, Head of Electrical Test Department, AITC Ghalam LLP, Astana, Kazakhstan; https://orcid.org/0009-0009-1037-1108; a.ivanov@ghalam.kz

Kelgenbayev, Almas Zhabaykhanuly – Engineer, Chief Engineer of Electrical test department, Ghalam LLP, Astana, Kazakhstan; https://orcid.org/0009-0000-2734-8988; a.kelgenbayev@ghalam.kz

Zhapanova, Ainur Shaizadanovna – Master (Sci.), Senior Lecturer at the Department of Radio Engineering, Electronics, and Telecommunications, S. Seifullin Kazakh Agrotechnical Research University, Astana, Kazakhstan; https://orcid.org/0009-0000-9012-2703; zhapanovaainur@gmail.com

Sailaubaiuly, Serikbol – Master (Sci.), Nazarbayev University, Astana, Kazakhstan; https://orcid.org/0009-0002-5597-2408; serikbolsailaubaiuly@gmail.com